Unexpected metabolic disorders induced by endocrine disruptors in *Xenopus tropicalis* provide new lead for understanding amphibian decline

Christophe Regnault[a,1], Marie Usal[a,1], Sylvie Veyrenc[a], Karine Couturier[b], Cécile Batandier[b], Anne-Laure Bulteau[c], David Lejon[d], Alexandre Sapin[d], Bruno Combourieu[d], Maud Chetiveaux[e], Cédric Le May[e], Thomas Lafond[f], Muriel Raveton[a], and Stéphane Reynaud[a,2]

[a]Univ. Grenoble-Alpes, Univ. Savoie Mont Blanc, CNRS, LECA, 38000 Grenoble, France; [b]Univ. Grenoble-Alpes, INSERM, LBFA, 38000 Grenoble, France; [c]Institut de Génomique Fonctionnelle de Lyon, Université Lyon 1, CNRS UMR 5242, Ecole Normale Supérieure de Lyon, 69000 Lyon, France; [d]Rovaltain Research Company, F-26300 Alixan, France; [e]Plate-forme Therassay, l'Institut du Thorax, INSERM, CNRS, Université de Nantes, 44007 Nantes, France; and [f]Centre de Ressources Biologiques Xénopes, Université Rennes 1, CNRS, Unité Mixte de Service 3387, 35042 Rennes, France

Edited by Vance L. Trudeau, University of Ottawa, Ottawa, ON, Canada, and accepted by Editorial Board Member David W. Schindler March 27, 2018 (received for review December 6, 2017)

Despite numerous studies suggesting that amphibians are highly sensitive to endocrine disruptors (EDs), both their role in the decline of populations and the underlying mechanisms remain unclear. This study showed that frogs exposed throughout their life cycle to ED concentrations low enough to be considered safe for drinking water, developed a prediabetes phenotype and, more commonly, a metabolic syndrome. Female *Xenopus tropicalis* exposed from tadpole stage to benzo(*a*)pyrene or triclosan at concentrations of 50 ng·L^{-1} displayed glucose intolerance syndrome, liver steatosis, liver mitochondrial dysfunction, liver transcriptomic signature, and pancreatic insulin hypersecretion, all typical of a prediabetes state. This metabolic syndrome led to progeny whose metamorphosis was delayed and occurred while the individuals were both smaller and lighter, all factors that have been linked to reduced adult recruitment and likelihood of reproduction. We found that F_1 animals did indeed have reduced reproductive success, demonstrating a lower fitness in ED-exposed *Xenopus*. Moreover, after 1 year of depuration, *Xenopus* that had been exposed to benzo(*a*)pyrene still displayed hepatic disorders and a marked insulin secretory defect resulting in glucose intolerance. Our results demonstrate that amphibians are highly sensitive to EDs at concentrations well below the thresholds reported to induce stress in other vertebrates. This study introduces EDs as a possible key contributing factor to amphibian population decline through metabolism disruption. Overall, our results show that EDs cause metabolic disorders, which is in agreement with epidemiological studies suggesting that environmental EDs might be one of the principal causes of metabolic disease in humans.

endocrine disruptors | metabolic syndrome | transgenerational | amphibian population decline | *Xenopus tropicalis*

Dramatic declines in amphibian wetland populations have been observed globally since the 1980s (1) with current extinction rates 211 times above background levels (2). It has been suggested that wetland pollution with multiple endocrine disruptors (EDs) may play a key role, along with other well-known threats including habitat loss, the introduction of exotic species, increased UV radiation, water acidification, and emerging infectious diseases (3–5). An ED is an exogenous substance or mixture that alters the function(s) of the endocrine system and consequently causes adverse health effects in an intact organism, or its progeny, or in (sub)populations (6). Mesoscale field studies have suggested that EDs may correlate with population decline in several amphibian species and that contamination by EDs may be one of the key contributing factors responsible for altering amphibian population fitness (7). While certain evidence suggests that once symptoms of ED toxicity are found in amphibian populations community destructuring and population decline are unavoidable (3), other studies have questioned these findings, suggesting that amphibians are no more vulnerable to EDs than other species (8). EDs have been extensively studied in vertebrates, focusing on their capacity to interfere with reproductive development and sex differentiation. Exposure to EDs at the larval stage can disrupt organogenesis and gonadal differentiation (9–15) by acting on cross talk between the thyroid and reproductive axes (16). Another sensitive phase is the breeding season during which adult frogs may develop egg and sperm maturation defects if exposed to EDs during critical stages (17–25). In addition to these developmental and reproductive effects, there are growing concerns that metabolic disorders might also

Significance

By performing a controlled exposure of an amphibian model to endocrine disruptors (EDs) at concentrations within the range of safe drinking water, we provide evidence of the role played by these widespread contaminants in amphibian population decline through metabolic disruption. In frogs exposed throughout their life cycle, this disruption induces a metabolic syndrome characteristic of a prediabetes state. Exposed animals produce progeny that metamorphose later, are smaller and lighter at the adult stage, and have reduced reproductive success. These transgenerational effects of EDs may impact overwintering survival, recruitment for reproduction, and fitness, each representing possible triggers of population decline.

Author contributions: M.R. and S.R. designed research; C.R., M.U., S.V., K.C., C.B., A.-L.B., D.L., A.S., B.C., M.C., C.L.M., T.L., and S.R. performed research; S.V. performed histological manipulations; K.C. and C.B. performed mitochondrial experimentations; A.-L.B. performed proteasome, aconitase, and citrate synthase experiments; D.L., A.S., and B.C. handled animal rearing and exposure; M.C. and C.L.M. performed plasma triglyceride measurements; T.L. performed *Xenopus* mating; M.R. participated in sample preparation; M.R. participated in data analyses; C.R., M.U., and S.R. analyzed data; and S.R. wrote the paper.

The authors declare no conflict of interest.

This article is a PNAS Direct Submission. V.L.T. is a guest editor invited by the Editorial Board.

Data deposition: The RNA-seq sequence data reported in this paper have been deposited at European Molecular Biology Laboratory–European Bioinformatics Institute, https://www.ebi.ac.uk/ena (accession no. PRJEB18463).

[1]C.R. and M.U. contributed equally to this work.

[2]To whom correspondence should be addressed. Email: stephane.reynaud@univ-grenoble-alpes.fr.

This article contains supporting information online at www.pnas.org/lookup/suppl/doi:10.1073/pnas.1721267115/-/DCSupplemental.

Published online April 23, 2018.

be linked to EDs (26). Data from epidemiological studies suggest that environmental EDs might account for a substantial part of metabolic disease incidence in humans (27–29). Despite these epidemiological correlations in humans and additional experimental evidence for mammals in general (30–32), the potential involvement of EDs in metabolic disorders as a possible cause of a reduction in fitness in amphibians has been largely neglected. The suspected ED (33) triclosan (TCS) has been shown to exert endocrine-disruptive effects on aquatic species through modulation of the thyroid and estrogen axes (34–37). In wetlands, this emerging contaminant can now be found alongside the well-known benzo(*a*)pyrene (BaP), which has been classified as an ED by several countries, including the United States and all European Union member countries, for its impact on reproduction

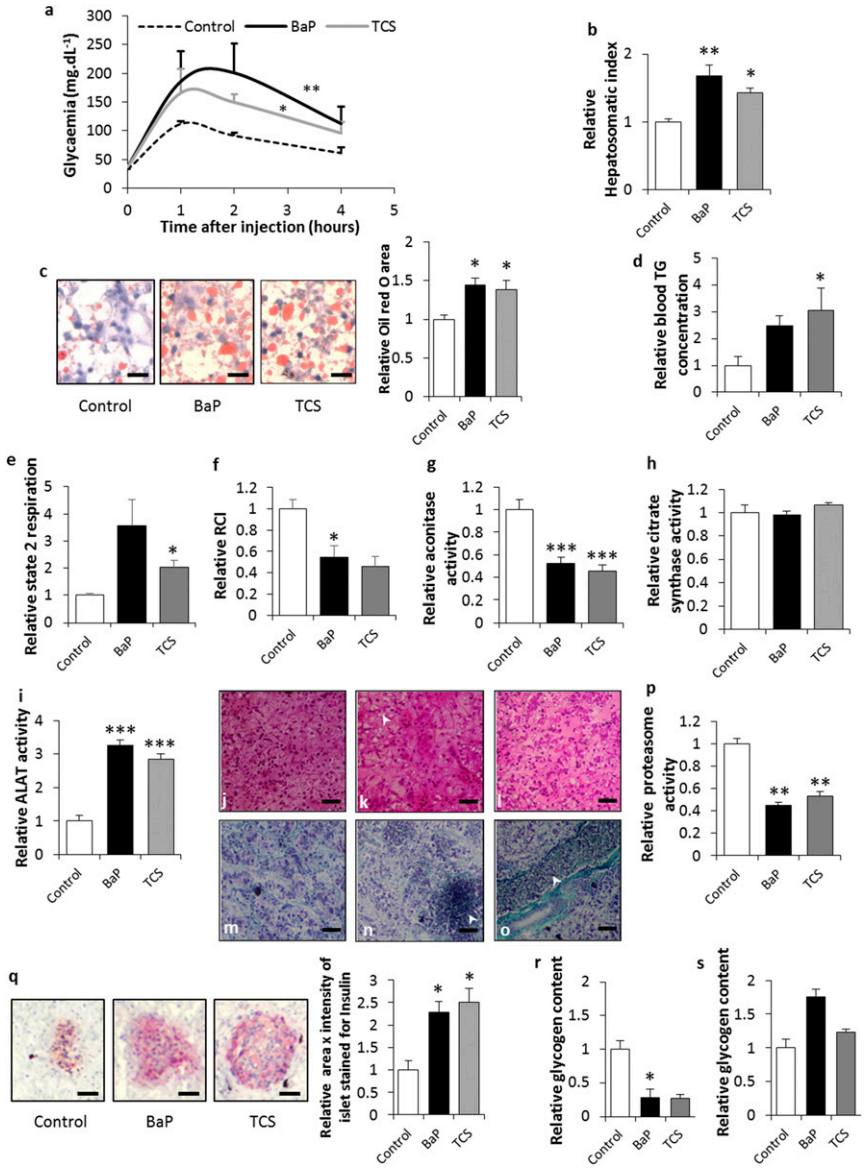

Fig. 1. ED exposure leads to metabolic impairments in *Xenopus*. (*A*) Glucose tolerance test. (*B*) Relative hepatosomatic indices of control and exposed animals. (*C*) Oil Red O staining for total lipid content measured in the livers of control and exposed animals. Lipid content is indicated by red staining. (Scale bars, 25 μm.) Histograms represent the relative Oil Red O area in the livers of control and exposed animals. (*D*) Relative blood triglycerides concentrations. (*E*) Relative mitochondrial state 2 respiration rate in liver of control and exposed animals. (*F*) Relative mitochondrial respiratory control indices in the livers of control and exposed animals. (*G*) Relative aconitase activity in control and exposed animals. (*H*) Relative citrate synthase activity in control and exposed animals. (*I*) Relative ALAT activity in control and exposed animals. (*J*) H&E stain of liver sections of control animals. (Scale bars, 70 μm.) (*K*) H&E stain of liver sections of BaP-exposed animals. The arrow indicates an area of ballooning hepatocytes. (Scale bars, 70 μm.) (*L*) H&E stain of liver sections of TCS-exposed animals. (Scale bars, 70 μm.) (*M*) Gomori's Trichrom stain of sections of control animals. (Scale bars, 70 μm.) (*N*) Gomori's Trichrom stain of liver sections of BaP-exposed animals. The arrow indicates a necrotic area with leukocyte infiltrates. (Scale bars, 70 μm.) (*O*) Gomori's Trichrom stain of liver sections of TCS-exposed animals. The arrow indicates a dilated blood vessel. (Scale bars, 70 μm.) (*P*) Relative proteasome activity in the livers of control and exposed animals. (*Q*) Insulin immunostaining of the pancreas of control and exposed animals. Insulin content is indicated by red staining. (Scale bars, 25 μm.) The histograms present the relative insulin quantity estimated as area × intensity of islet stained for insulin in the pancreas of control and exposed animals. (*R*) Relative glycogen content in the muscles of control and exposed animals. (*S*) Relative glycogen content in the livers of control and exposed animals. The statistical analysis was performed using Dunnett's test on log-transformed data. The asterisks indicate a significant difference from the control: $*P < 0.05$, $**P < 0.01$, $***P < 0.001$; $n = 4$ per exposure group.

(38, 39). Recent studies have demonstrated that acute exposure to BaP and TCS (10 $\mu g \cdot L^{-1}$, during 24 h) can induce marked metabolic disorders in female and male *Xenopus tropicalis* with an insulin resistance-like (IR) syndrome phenotype and hepatotoxicity due to impaired lipid metabolism (40, 41). However, the precise impact of EDs at naturally occurring concentrations on the amphibian metabolism, their health, and decline are unknown. Given that BaP and TCS concentrations in contaminated surface water (including lakes and ponds) vary from 0.1 to 237 $ng \cdot L^{-1}$ (42, 43) and 0.8–74 $ng \cdot L^{-1}$ (44, 45), respectively, the impact of these chemicals must be studied within this concentration range, using a transgenerational approach to prove their involvement in reduced amphibian fitness.

Here, we report on the real impact of EDs on amphibian metabolism and the consequences for their fitness by investigating two widespread EDs, BaP and TCS (40, 41), at environmental concentrations (50 $ng \cdot L^{-1}$) that are considered safe for human consumption (46, 47). Exposing female *Xenopus* to BaP and TCS from tadpole to mature adult stage (for 12 mo) led to a hepatic transcriptomic signature as well as liver, muscle, and pancreatic physiological impairments typical of a prediabetes state. With BaP exposure the observed metabolic syndromes had not been reversed after 1 y of depuration in clean water. In addition, exposed animals displayed a dramatic reduction in reproductive success, and produced progeny (F_1) with a decreased capacity to reproduce and produce viable progeny (F_2). These data provide insights into transgenerational effects and suggest that EDs may have a direct causal relationship with amphibian population decline by disrupting their energy metabolism.

Results and Discussion

Development of ED-Exposed Animals (F_0). BaP- and TCS-exposed animals showed a significantly delayed metamorphosis (the 90% population metamorphosis level was reached 21 and 31 d later, respectively) (Fig. S1*A*) while exhibiting no significant decrease in size or weight at the time of metamorphosis (Fig. S1 *B* and *C*). Moreover, the time to reach sexual maturity was unaffected in exposed females (Fig. S1*D*).

EDs Induce a Marked Metabolic Syndrome in *Xenopus* Typical of a Prediabetes State. No difference in basal serum glucose levels was found between the exposed and control animals. However, ED exposure led to a reduction in glucose tolerance with a 1.8- to 2.4-fold increase in blood glucose (Fig. 1*A*). Investigating the liver physiology showed that the ED-exposed animals that had become glucose intolerant displayed an increase in their hepatosomatic index, co-occurring with a marked hepatic steatosis (Fig. 1 *B* and *C*). This deregulation of lipid metabolism in the liver was associated with hypertriglyceridemia (Fig. 1*D*). Mitochondria orchestrate the energy metabolism from lipids through substrate oxidation via β-oxidation (48), and mitochondrial dysfunction has been associated with chronic liver steatosis (30). Here, an elevated state 2 respiratory rate in combination with a decreased respiratory control index (RCI) pointed toward a mitochondrial uncoupling in exposed animals (Fig. 1 *E* and *F*). Fatty liver and mitochondrial uncoupling have been associated with oxidative stress (48). A general deficit in Fe–S cluster proteins such as aconitase, a tricarboxylic acid cycle mitochondrial enzyme that contains a 4F–4S cluster as prosthetic group, is a phenotype commonly associated with oxidative stress in the mitochondria (49). Our results suggest that ED exposure induces elevated mitochondrial rates of free radical production that result in aconitase inactivation (Fig. 1*G*). In addition, since the citrate synthase activity remained stable, irrespective of treatment type (Fig. 1*H*), the aforementioned changes in the mitochondrial parameters were not associated with variations in mitochondrial density in the liver. Taken together, our results suggest that liver steatosis induced by EDs is linked to mitochondrial dysfunction and, specifically, to mitochondrial uncoupling associated with oxidative stress.

Liver lipid accumulation has been widely associated also with hepatoxicity (50). ED-exposed *Xenopus* displayed a 2.8–3.2 increase in serum activity of alanine aminotransferase (ALAT) (Fig. 1*I*) and liver necrosis associated with pronounced tissue disorganization. Under magnification, the liver tissue in exposed *Xenopus* showed hepatocytes with fewer cell contacts and irregular shapes, together with large areas of necrosis (Fig. 1 *J*–*O*). Proteasome dysregulation has been associated with endoplasmic reticulum (ER) stress and is the primary event of insulin resistance development (51). Here, we found that ED exposure induced a twofold decrease in liver proteasome activity (Fig. 1*P*), suggesting that general insulin resistance syndromes occur regardless of the pollutant studied. This development of insulin resistance syndrome in ED-exposed *Xenopus* is supported by the twofold increase in insulin production by the pancreatic beta cells (Fig. 1*Q*). In type 2 prediabetes, an increased metabolic demand for insulin due to insulin resistance precedes the onset of hyperglycemia. This leads to a period of normal glycaemia, during which the pancreatic beta cells compensate for insulin resistance by hypersecreting insulin (52). Nonalcoholic fatty liver disease (NAFLD) and its progression to nonalcoholic steatohepatitis (NASH) are hepatic signs of metabolic disorders including prediabetes and insulin resistance syndrome. Histological modifications associated with NAFLD/NASH include steatosis, inflammation, hepatocellular ballooning, and fibrosis (53). The liver sections of ED-exposed animals presented severe steatosis, leukocyte infiltrates, and hepatocyte ballooning, especially in BaP-treated animals (Fig. 1 *K* and *N*). TCS-exposed animals displayed swollen blood vessels typical of NAFLD (54) (Fig. 1*O*). The severity of the histopathological phenotypes observed suggests that TCS-exposed animals presented livers with modifications typical of NAFLD, and that BaP-exposed *Xenopus* presented livers with modifications typical of progression to NASH. However, regardless of the liver sections considered, and despite the large areas of necrosis, no fibrosis was observed in BaP-exposed frogs (Fig. 1*N*). In addition to the liver, pancreatic, and blood phenotypes, we also observed a decrease in muscle glycogen content for ED-exposed animals (Fig. 1*R*) suggesting an insulin resistance syndrome in the skeletal muscle (55). Taken together, our results suggest that ED exposure may lead to a prediabetes phenotype and, more generally, to the development of general metabolic syndrome in frogs exposed throughout their life cycle. Moreover, we observed a trend toward an increase in the liver glycogen content in BaP-exposed animals (Fig. 1*S*). These results point toward a possible association of this metabolic syndrome with a glycogenic hepatopathy, in humans considered a complication of uncontrolled diabetes (56).

Liver Transcriptomic Signatures in ED-Exposed Animals Confirm Metabolic Syndrome. Liver transcriptomes of ED-exposed animals showed a differential transcription of 322 and 121 genes with up-regulation in 40% and 66% of cases for BaP and TCS, respectively (Datasets S1 and S2). Despite having a similar prediabetes phenotype, the liver transcriptomic signatures varied for different treatments. Kyoto Encyclopedia of Genes and Genomes (KEGG) pathway enrichment analyses of the differentially transcribed genes indicated a link between BaP treatment and "Metabolic pathways" (2.9-fold), "Biosynthesis of amino acids" (3.5-fold), "Steroid hormone biosynthesis" (3.7-fold), "Peroxisome" (3.7-fold), "Chemical carcinogenesis" (3.8-fold), "Carbon metabolism" (3.8-fold), "Metabolism of xenobiotics by cytochrome P450" (4.1-fold), "Glycine, serine and threonine metabolism" (7.8-fold), "Glyoxylate and dicarboxylate metabolism" (eightfold), "Protein export" (13.2-fold), and "Protein processing in endoplasmic reticulum" (5.4-fold) (Fig. 2*A*).

For TCS exposure, a significant enrichment was observed for "FoxO signaling pathway" (3.7-fold), "Protein processing in endoplasmic reticulum" (3.4-fold), "Metabolism of xenobiotics by cytochrome P450" (7.4-fold), and "Chemical carcinogenesis" (7.1-fold) (Fig. 2*A*). The "Metabolism of xenobiotic by cytochrome P450" and "Chemical carcinogenesis" pathway enrichments, found for both EDs, did not correlate with the differential transcriptions of genes involved in BaP and TCS metabolism or bioactivation, which suggests that the frogs' strategy for xenobiotic protection may not be linked to the induction of biotransformation activities (40, 41) (Fig. 2*B* and Datasets S1 and S2).

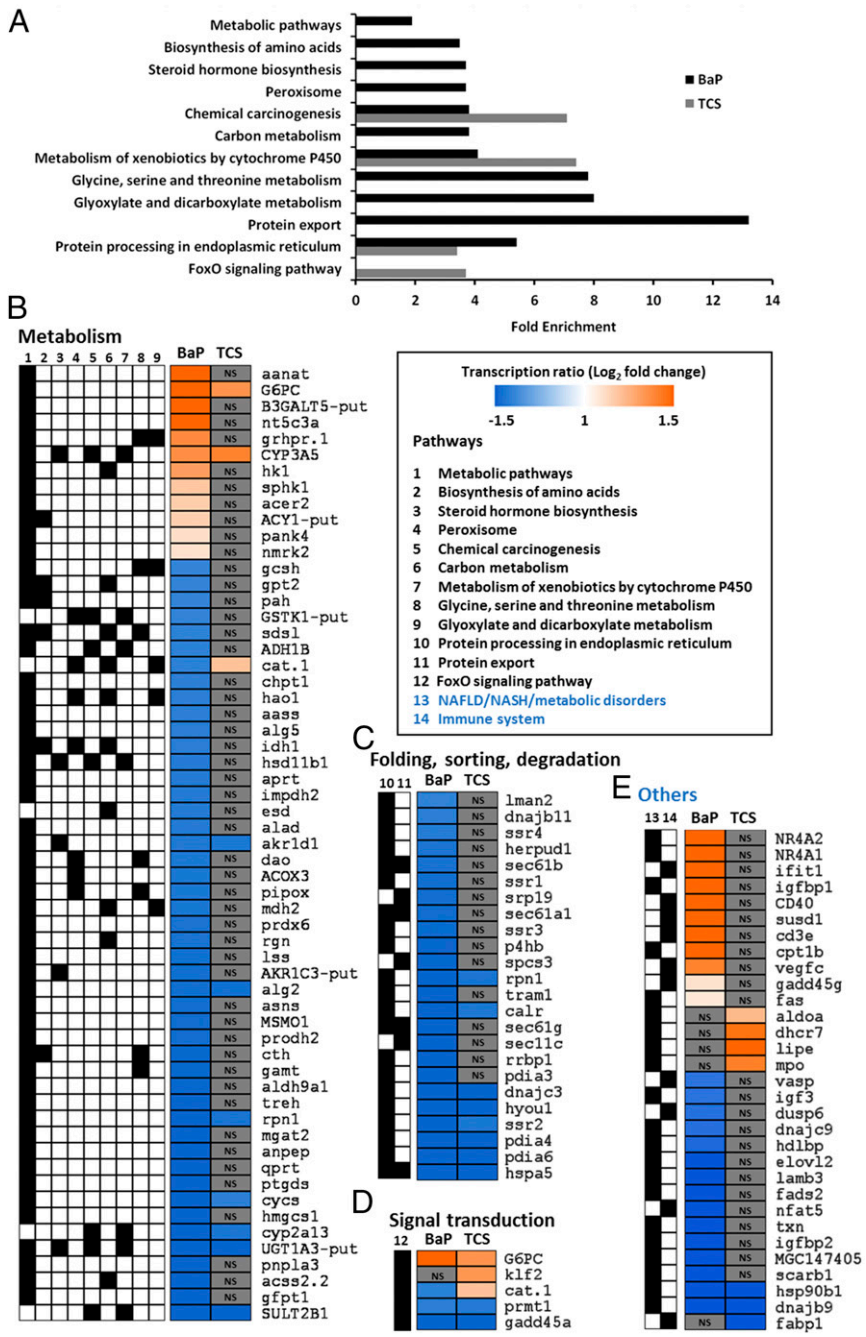

Fig. 2. Liver transcriptome following ED exposure indicates a marked metabolic impairment typical of IR syndrome. (*A*) The genes showing a significant differential transcription from control in at least one condition were used for annotation enrichment using the Database for Annotation, Visualization and Integrated Discovery (DAVID) functional annotation tool (modified Fisher's exact test with $P < 0.05$). Histograms indicate the level of enrichment of the pathways, whenever the levels were significant for BaP- or TCS-exposed animals. (*B–D*) Transcription of genes involved in the different pathways. The color scale indicates transcription ratios relative to the controls. The black boxes indicate the pathway highlighted by the gene found to be differentially transcribed compared with the control. Pathways have been grouped according to their parent root in the KEGG description. (*E*) Transcription of genes involved in the immune system or where a literature search yielded specific links with the NAFLD/NASH syndrome. The black boxes indicate the pathway highlighted by the gene found to be differentially transcribed compared with the control. NS indicates that the specific gene was not found to be differentially transcribed in the considered exposure with regard to the control. $n = 4$ per exposure group.

Chronic ER stress due to the accumulation of unfolded proteins in the liver has been described in various models of NAFLD (57). Here, we found a marked enrichment of the pathways linked to protein processing and export, highlighted by a decrease in ED-exposed animals in the transcription of gene coding for proteins involved in adaptive unfolded protein response (UPR) (*hspa5*, *dnajc3*, *dnajc9*, *dnajb9*, *dnajb11*, *pdia4*, *hsp90b1*, *calr*; Fig. 2 *C* and *E* and Datasets S1 and S2). Since ER stress has been linked to the inhibition of proteasome activity (51), the adaptive UPR response was most likely inhibited by the frogs' exposure to EDs. This type of inhibition has been linked to cell death (58) and explains the large areas of necrosis observed in the liver sections of BaP-exposed animals (Fig. 1*N*).

All other enriched pathways considered together suggest that an IR phenotype occurs in *X. tropicalis* exposed to EDs. These other pathways mainly involve genes linked to carbohydrate or lipid metabolism (Fig. 2 *B* and *D*). In addition, we found several differentially transcribed genes for which a deregulation has also been associated with IR and NAFLD/NASH (Fig. 2*E*). IR is characterized by an increase in the enzyme-coding transcripts involved in gluconeogenesis such as glucose-6 phosphatase (*g6pc*) or glyoxylate reductase (*grhpr.1*) (59, 60), and we did indeed find a marked overtranscription of the *g6pc* (6.8-fold for BaP and 2.5-fold for TCS) and *grh.1* (2.6-fold for BaP) genes. Moreover, the high overtranscription of the insulin-like growth factor 1 binding protein (*igfbp-1*), repressed by insulin in physiological conditions (61), confirmed this phenotype for BaP-exposed *Xenopus* (Fig. 2 *B* and *E*). The high activation of gluconeogenesis in BaP-exposed animals might be related to the high overtranscription of the nuclear receptors *nr4a1* (6.7-fold) and *nr4a2* (14-fold), which are key activators of glucose production in the liver (62) (Fig. 2*E*).

The IR syndrome has also been associated with a deregulation of lipid metabolism, leading to the accumulation of triglycerides (steatosis) in the liver (63). The marked liver steatosis in our ED-exposed animals was linked to the deregulation of several genes controlling lipid metabolism, and particularly sulfotransferase 2b1 (*sult2b1*), an enzyme known to protect the liver from steatosis and to inhibit lipogenesis (64), was undertranscribed (0.21-fold for BaP and 0.35-fold for TCS). Moreover, BaP-exposed animals presented a deregulation of patatin-like phospholipase domain containing 3 (*pnpla3*) (0.26-fold), the gene whose inhibition has been associated with lipid accumulation in the liver (65). In TCS-exposed animals, several genes associated with liver triglyceride or cholesterol accumulation were found to be overtranscribed, including the 7-dehydrocholesterol reductase (*dhcr7*) (2.75-fold) and the Kruppel-like factor 2 (*klf2*) (2.52-fold) (41, 66).

The aforementioned physiological observations indicated a graduation in liver manifestations of IR in ED-exposed animals, with liver symptoms ranging from NAFLD for TCS-exposed to NASH in BaP-exposed *Xenopus* (Fig. 1). Transcriptomic data confirmed these phenotypes with a higher number of genes highlighting the severity of liver dysfunction under BaP exposure. We did indeed find a marked undertranscription of several genes involved in lipid metabolism (*acss2.2*, 0.24-fold; *elovl2*, 0.35-fold; *hmgcs1*, 0.31-fold; *mgat2*, 0.34-fold), the deregulation of which has been associated with the progression from NAFLD to NASH (67). NASH has also been found to be associated with inflammatory processes (53), which is in good agreement with our observation of leukocyte infiltrates in BaP-exposed animals being associated with the deregulation of key genes involved in inflammation, including *cd3e* (3.15-fold), *cd40* (3.34-fold), *fas* (2.11-fold), *gadd45g* (2.15-fold), *susd1* (3.15-fold), *vasp* (0.48-fold), and *vegfc* (2.75-fold). The different liver transcriptomic signatures induced by BaP and TCS might be explained by their different cellular targets. The BaP phenotype could be induced through Ah-R activation, since this nuclear receptor has been shown to be involved in NAFLD/NASH and liver inflammatory processes in mice (68). In mammals, TCS has been described as activating the pregnane and xenobiotic receptor (PXR) (69). In turn, this receptor has been found to be involved in NAFLD in the absence of any inflammatory processes (70), which could explain the liver metabolism deregulation induced by TCS. However, further studies are required to conclusively elucidate the underlying causes of these observed similarities and differences in ED-activated molecular mechanisms and the resulting metabolic syndrome.

BaP-Induced Metabolic Syndrome and Glucose Intolerance Are Irreversible. To examine the reversibility of the observed symptoms, we performed a 1-y depuration of the exposed animals. While the glucose intolerance phenotype appeared reversible in TCS-exposed *Xenopus*, individuals exposed to BaP remained glucose intolerant even after 1 y of depuration in clean water (Fig. 3*A*). Moreover, the BaP depurated animals still displayed a marked increase in their hepatosomatic index, linked with hepatic steatosis, while TCS-exposed animals only showed the liver steatosis (Fig. 3 *B* and *C*). These hepatic manifestations were accompanied by an insulin secretory defect, especially for BaP-exposed animals (Fig. 3*D*). However, since only the BaP-exposed animals remained glucose intolerant, our results suggest that the liver damage induced by this ED is irreversible.

ED-Induced Metabolism Impairments Reduce Fitness and Cause Multigenerational Effects. EDs at natural concentrations induced a marked metabolic impairment in female *Xenopus*, on which the resources found in the eggs are entirely dependent (71). To test the effects of parental exposure on their progeny, we mated five pairs that had been exposed to either of the EDs (BaP or TCS), which resulted in offspring from all five BaP exposed pairs but only from two that had been exposed to TCS. Despite their sexual maturity, three out of five TCS-exposed females did not accept the male, which suggests that TCS may impair sexual behavior in amphibians. This had already been observed in fish (72) and would confirm the capacity of TCS to impair the hypothalamo-pituitary-gonad axis (36).

Although the progeny had not directly been exposed to EDs, they showed a significantly delayed metamorphosis (by 35 d for 90% of the population to reach frog metamorphosis) (Fig. 4*A*), just like their BaP-exposed genitors, demonstrating the multigenerational impact of EDs. Moreover, BaP-exposed parents produced F_1 individuals that were smaller and lighter, while TCS exposed parents produced offspring that was just lighter (Fig. 4 *A* and *B*), demonstrating a multigenerational aggravation of the phenotype observed in their genitors.

For the case of direct exposure to TCS, the observed developmental effects may be due to TCS's immediate impact on thyroid hormone levels (73), while BaP exposure may cause indirect effects through Ah-R cross talk with the thyroid hormone receptor (74). However, since F_1 animals were exposed to EDs only at the gamete stage, a similar explanation for the observed transgenerational impacts is less obvious. This effect could be explained by a decrease in egg resources due to the observed metabolic impairments in the female genitors, or an ED exposure-induced epigenetic modification of genes controlled by thyroid hormones. Irrespective of the underlying cause, these disturbances could play a major role in the ongoing amphibian population decline as the delayed metamorphosis, together with their smaller body size at the time of metamorphosis, reduces their adult recruitment and chances for successful reproduction (75). The smaller body size at the time of metamorphosis also limits food availability for the newly metamorphosed frogs because of gape limitation, while increasing their vulnerability to gape-limited predators (76). The smaller initial body size possibly also reduces postmetamorphic growth, which in turn impacts

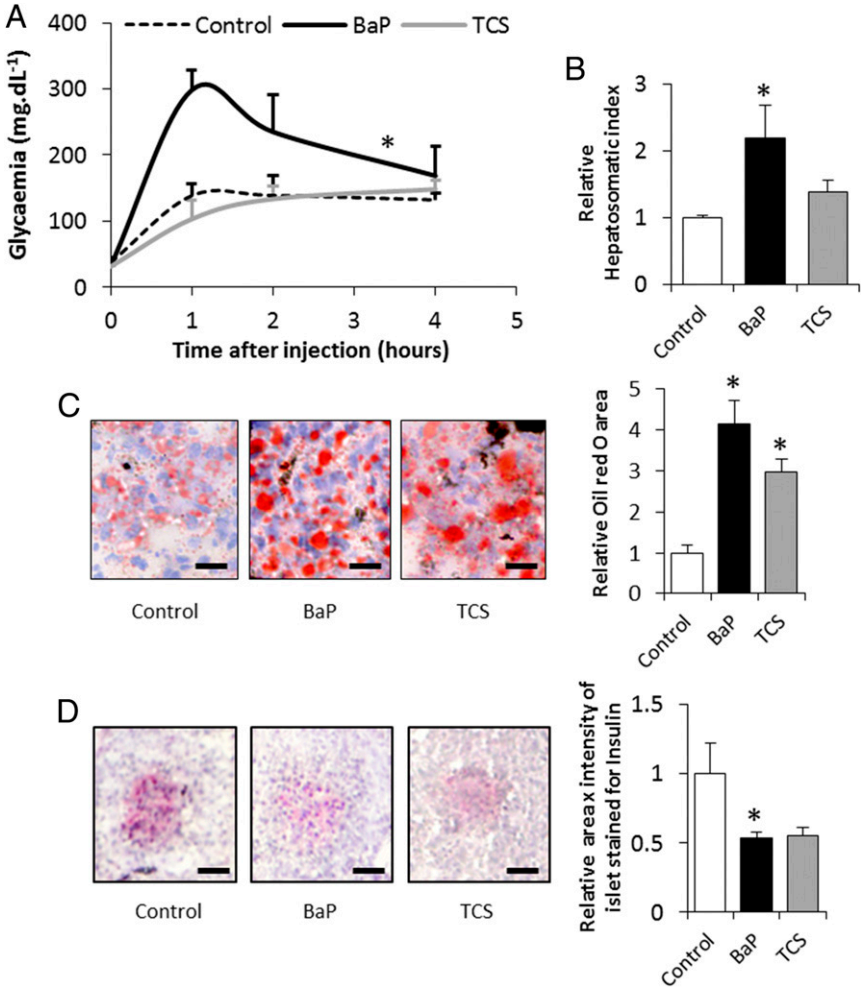

Fig. 3. Persistence of metabolic impairments in *Xenopus* after 1 y of depuration. (*A*) Glucose tolerance test. (*B*) Relative hepatosomatic indices of control and exposed animals. (*C*) Oil Red O staining for total lipid content measured in the livers of control and exposed animals. Lipid content is indicated by red staining. (Scale bars, 25 μm.) Histograms present the relative Oil Red O area in the livers of control and exposed animals. (*D*) Insulin immunostaining of the pancreas of control and exposed animals. Insulin content is indicated by red staining. (Scale bars, 25 μm.) The histograms show the relative insulin quantity estimated from the product of area × intensity of the islet stained for insulin in the pancreas of control and exposed animals. The statistical analysis was performed using Dunnett's test on log-transformed data. The asterisk indicates a significant difference from the control: $*P < 0.05$; $n = 3$ per exposure group.

on their overwintering survival rates. The reduced body size particularly affects females as their size is directly proportional to fecundity (77). We found that F_1 females from BaP-exposed genitors reached sexual maturity 141 d later than the control (90% of all females having reached maturity) (Fig. 4*C*). To assess F_1 reproductive success and the fitness of their exposed genitors, we mated five F_1 pairs from the control, five F_1 pairs from the BaP-exposed parents group, and one pair with TCS-exposed genitors (corresponding to the only two surviving adults from this group). We observed a disturbance in mating behavior for both ED groups, characterized by a delayed amplexus formation. At 3 h poststimulation, only two amplexi were successful for F_1 with BaP parental exposure, while the one pair with TCS parental exposure remained unsuccessful (Fig. 4*E*). Irrespective of parental exposure, F_1 mating resulted in a highly variable number of hatched eggs, although with a discernible trend indicating dramatically fewer hatched eggs from F_1 individuals with BaP- and TCS-exposed parents (Fig. 4*F*), suggesting reduced fitness induced by ED exposure.

In this work, we focused on finding links between ED exposure and amphibian population decline. In agreement with epidemiological studies in humans (27–29), we found that EDs can induce severe metabolic disorders in amphibians already at concentrations that would be considered safe for higher vertebrates. Moreover, parental exposure to EDs can negatively affect the development and fecundity of their progeny and thus reduce fitness. Overall, the findings from this study should serve as a starting point for future studies to further elucidate the role of EDs as a contributing cause to amphibian population decline, particularly through their disruption of the energy metabolism. Our results also provide insights into the transgenerational effects of EDs, which may apply not only to amphibians but also to higher vertebrates including humans.

Methods

Animals. Premetamorphic, 7-d-old *Xenopus tropicalis* were purchased from the "*Xenopus* national husbandry" (CRB "Xenopes"), University of Rennes 1 (https://xenopus.univ-rennes1.fr/). Before the experiments, they were allowed to acclimate for 1 wk at 25 °C with a photoperiod of 12:12 h in Marc's modified Ringer's (MMR) 0.1× medium (pH 7.4; NaCl, 10 mM; KCl, 2×10^{-1} mM; $MgSO_4$, 10^{-1} mM; $CaCl_2$, 2×10^{-1} mM; Hepes, 5×10^{-1} mM). The frogs were fed daily ad libitum with finely ground pellets of trout food (Aquatic 3; Special Diets Services), and the grinding level was continually adjusted to the size of their jaw. At an age of 2 wk, the density of young tadpoles was 50 individuals per 2 L of medium, distributed in two tanks per exposure

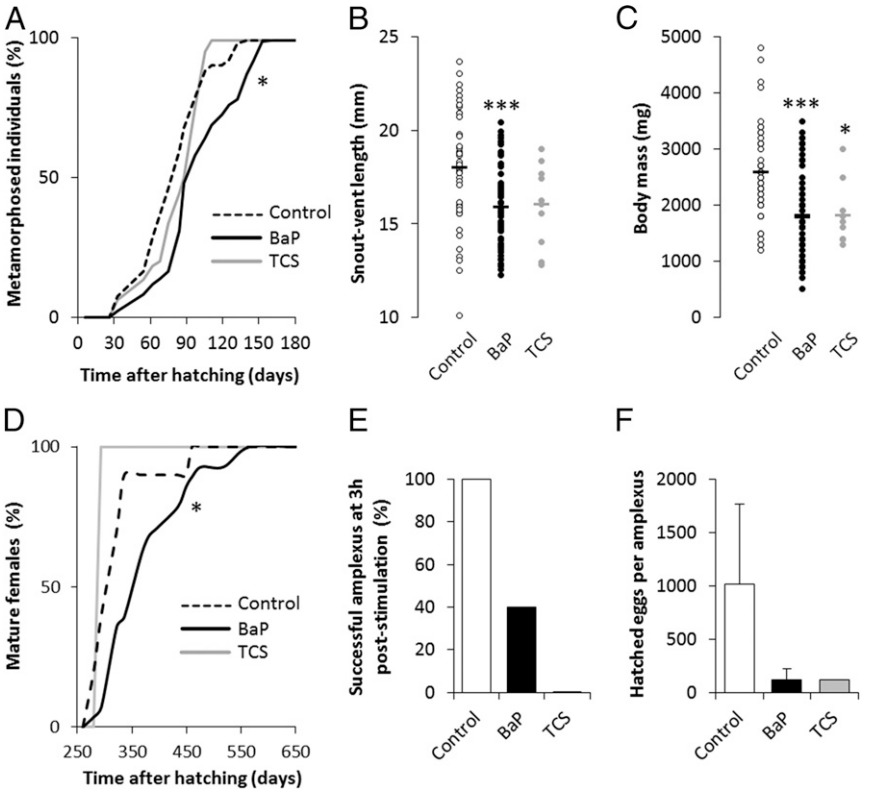

Fig. 4. Parental exposure to EDs leads to delayed metamorphosis and reduced size and weight of progeny. (*A*) Development curves of F_1 individuals from hatching to metamorphosis. The distributions of F_1 individual development times were compared between the control and each parental ED-exposed population using a Kaplan–Meyer test to evaluate global curve difference. The asterisk indicates a significant difference from the control: $*P < 0.05$ (n = 716, 1,020, and 72 for control, BaP, and TCS parental exposure). (*B*) Snout-vent length of F_1 individuals at time of metamorphosis from each parental exposure group. (*C*) Weight of F_1 individuals at time of metamorphosis from each parental exposure group. The statistical analysis was performed using Dunnett's test on log-transformed data. The asterisks indicate a significant difference from the control: $*P < 0.05$, $***P < 0.001$ (n = 46, 63, and 10 for control, BaP, and TCS parental exposure, respectively). (*D*) Development curves of F_1 juvenile females from hatching to sexual maturity. The distributions of F_1 individual development times were compared between the control and each parental ED-exposed population using a Kaplan–Meyer test to evaluate global curve difference. The asterisk indicates a significant difference from the control: $*P < 0.05$ (n = 10, 28, and 1 for control, BaP, and TCS parental exposure). (*E*) Percentage of successful amplexus 3 h poststimulation of F_1 animals (n = 5, 5, and 1 for the control, BaP, and TCS parental exposures, respectively). (*F*) Number of hatched eggs per F_1 female from each successful amplexus (n = 5, 5, and 1 for the control, BaP, and TCS parental exposures, respectively).

condition (see below). Once they had reached 30 d, that is, immediately before undergoing metamorphosis, the frogs were moved to larger tanks with 4 L of medium (30 individuals per tank) to meet their increased volume requirements. Once metamorphosis was complete, that is, at age 150 d, the *Xenopus* were dispatched into four tanks at a density of 10 individuals per 4 L of medium. All experiments were performed in an animal house accredited by the French Ministry of Animal Welfare (Rovaltain Research Company; no. A 26 004 1401) and in accordance with the recommendations of the ethics committee ComEth Grenoble–C2EA–12 (animal welfare agreement no. 02545.03).

***Xenopus* Exposure to BaP and TCS.** *Xenopus* were exposed collectively at 25 °C in their tanks using 150 tadpoles per condition. One-quarter of the medium was renewed daily and completely renewed once per week using a solution of MMR containing either BaP (97% purity; Sigma-Aldrich) or TCS (97% purity; Sigma-Aldrich) at an initial concentration of 200 $ng{\cdot}L^{-1}$. The control frogs were exposed to dimethyl sulfoxide (DMSO) (vehicle) at a concentration of 4/1,000 (vol/vol). Pollutant concentrations in the medium we continually monitored by GC-MS/MS. Freshly prepared media (either with BaP, TCS, or DMSO) were placed in identical tanks, with identical light, temperature, and *Xenopus* densities for the different exposure experiments. Analyses showed that 85% of BaP and 87% of TCS were usually absorbed within 24 h, which, considering the periodical medium renewals, equates to a weekly average concentration of 50 $ng{\cdot}L^{-1}$. These concentrations were chosen to match the BaP or TCS concentrations usually found in "naturally" polluted waters (42–45), and particularly for BaP, this concentration is still below the recommended critical threshold and thus considered safe for human drinking (46, 47). At the time of writing, no equivalent critical threshold had been published for TCS.

After 12 mo of exposure, four females from each exposure condition underwent a glucose tolerance test. Eight others (divided in two groups of four to ensure sufficient material for all of the experiments) were rapidly killed with a blow to the head and immediately dissected to sample the liver, the pancreas, and the muscles. Blood was collected by means of an intracardiac puncture. To mimic a depuration period, three females from each exposure condition were transferred to clean medium and maintained for 12 mo, after which the organ sampling was carried out as described above.

Hepatosomatic Index. Each *Xenopus* and their liver were weighed to the nearest 0.1 mg, and the hepatosomatic index (HSI) was calculated as follows:

$$HSI = (\text{liver weight}[g]) \times (\text{total body weight}[g])^{-1} \times 100.$$

Histological Observations. After dissection, the liver (same lobe/frog) and pancreas were embedded in Tissue OCT (Labonord; VWR), immediately flash frozen in liquid nitrogen, and conserved at −80 °C. Transverse sections (7 μm) were produced using a cryostat (CM3050 S; Leica) with the temperature of the cryochamber and specimen set to −25 °C. Frozen sections were mounted on Super-Frost Plus microscope slides (Labonord).

The frozen sections of the liver were stained with Oil Red O to assess total lipid hepatic content as previously described (41).

Hepatic glycogen content was estimated using periodic acid–Schiff (PAS) staining. The slides were briefly rinsed in water and incubated with 0.5% periodic acid for 10 min before staining with Schiff reagent for 15 min and

hematoxylin for 1 min. The sections were dehydrated by 1-min incubation in 70% ethanol, followed by 1-min incubation in 95% ethanol, followed by 1-min incubation in toluene. PAS scoring was performed by two people independently. The PAS staining score (0–4) was assigned depending on the percentage of glycogen in the cells with a score of 0 corresponding to no glycogen and a score of 4 corresponding to a cell full of glycogen.

Frozen pancreas sections were fixed for 10 min in 4% formaldehyde and washed in PBS containing 0.5% BSA. A saturation step was performed for 30 min in PBS containing 5% BSA. The sections were then incubated overnight at 4 °C with guinea pig anti-human insulin serum (Y370; Yanaihara Institute) diluted 1:500 in PBS–BSA (0.5%). The sections were then washed again in PBS–BSA (0.5%) and incubated with goat anti-guinea pig IgG (H+L) FITC-conjugated (SouthernBiotech), diluted 1:200 in PBS–BSA (0.5%), and left for 30 min at room temperature in the dark. We used the Converter AP (Roche) on the frozen sections according to the manufacturer's instructions to convert the fluorescence into a colorimetric signal. Revelation was performed using Fast Red (Sigma-Aldrich) as substrate for 15 min. After labeling, the frozen sections were counterstained with Mayer's Haemalun (Merck) and mounted with aqueous mounting medium (aquatex; Merck). Each slide (one per animal) was photographed under a Nikon Eclipse E600 microscope using an Olympus DP70 digital camera. Five pictures were taken, corresponding to the five insulin hot spots, labeled by section. Each picture was imported into the GNU Image Manipulation Program (GIMP, version 2.8.6), where the area of each labeling acini was quantified using the built-in histogram function. Because insulin appeared magenta on the pictures, the labeling intensity was estimated from the inverse of the green channel level, again using the histogram dialogue. For each slide, this intensity was quantified as previously described (41) and used to standardize acini intensity. Insulin production was obtained by multiplying the acinus area with the standardized labeling intensity for each acinus.

Hepatic Mitochondrial Respiration. The mitochondria were prepared as described in Garait et al. (78) (isolation medium: pH 7.4, 250 mM sucrose, 20 mM Tris, 1 mM EGTA). Mitochondrial protein concentration was determined according to the manufacturer's instructions with a Pierce modified Lowry protein assay (Thermo Fisher Scientific). The mitochondrial oxygen consumption rate was measured polarographically with a Clark oxygen electrode in a closed and stirred glass cell. The respiration medium (pH 7.2, 125 mM KCl, 20 mM Tris, 5 mM Pi, 1 mM EGTA) was supplemented with 5 mM glutamate, 2.5 mM malate, and 5 mM succinate for measuring complex I and complex II-mediated mitochondrial respiration (state 2). State 3 respiration was measured after the addition of 500 mM ADP, and the RCI was defined as the following ratio: state 3/state 2.

Liver Proteasome Activity. Peptidase activity of the proteasome was assayed using a fluorogenic peptide, succinyl-Leu-Leu-Val-Tyr-7-amido-4-methylcoumarin (LLVY-AMC) (Sigma-Aldrich), as previously described (79).

Liver Aconitase Activity. Mitochondria were suspended in 25 mM phosphate buffer, pH 7.25, supplemented with 0.05% Triton X-100, and aconitase activity was assayed spectrophotometrically at 340 nm, as previously described (49).

Liver Citrate Synthase Activity. Citrate synthase activity was measured as the rate of appearance of thionitrobenzoic acid, followed by an increase in absorbance at 412 nm during 3 min in the presence of 10 μg of isolated mitochondria protein, 100 mM Tris·HCl, pH 8.0, 0.1% Triton X-100, 300 mM acetyl-CoA, 100 μM 5,5′-dithiobis-(2-nitrobenzoic acid), and 500 μM oxaloacetate.

Muscle Glycogen Content. Forty milligrams of muscle were lysed in 40% KOH at 100 °C during 30 min before cooling and overnight glycogen precipitation with 100% ethanol at −20 °C. After centrifugation at 10,000 × *g* for 15 min at 4 °C, the glycogen pellet was hydrolyzed in glucose by incubation in 2 M HCL at 100 °C for 3 h. After neutralization with 2 M NaOH, the concentration of glucose was measured with the GAGO-20 kit (Sigma-Aldrich), following the manufacturer's instructions.

Glucose Tolerance Test. Blood glucose was measured by digital sampling, 0, 1, 2, and 4 h after glucose injection in the dorsal lymph sac (1 mg·g^{-1} fresh mass) using a hand-held plasma calibrated glucometer (Accu-Chek Performa; Roche Diagnostics). The area under the curve after the glucose challenge was used for the statistical comparison.

ALAT Activity in the Serum. Serum was obtained from fresh-blood centrifugation (3,000 × *g* for 10 min at 4 °C) and stored at −80 °C. ALAT activity was measured using 3 mL of pure *Xenopus* serum, according to the manufacturer's instructions (Alanine Aminotransferase Activity Assay Kit; Sigma-Aldrich).

Plasma Triglyceride Measurements. Plasma total triglyceride concentrations were determined using a triglycerides GPO-PED kit (Sobioda).

Statistics. For F_0, individual data are expressed as the mean ± SEM. The values were derived from four individual experiments for frogs immediately killed after 12 mo of exposure and from three individual experiments for frogs killed after 12 mo of depuration postexposure. Since the statistical distribution of the replicates was unknown (Gaussian or not) for four or three replicates, the comparison of each treatment (either BaP or TCS) with a single control was performed using the many-to-one comparison test of Dunnett (80, 81) after log-transforming the data.

The distributions of F_0 and F_1 individual development times were compared between the control populations and each parental ED-exposed population separately, using a Kaplan–Meyer test to evaluate global curve differences.

The distribution of F_0 and F_1 female maturity time between control populations and each parental ED-exposed population was determined separately, using a Kaplan–Meyer test to evaluate global curve differences.

For snout-vent length and weight of F1 individuals, since the nature of the distribution of the results was not Gaussian for TCS parental exposure, the comparison of each parental treatment (either BaP or TCS) with a single control was performed using the many-to-one comparison test of Dunnett (80, 81) after log-transforming the data.

Liver RNA Extraction and Sequencing. For each biological replicate, total RNA was extracted from 15 mg of liver using the RNAqueous-4PCR Kit (Ambion), according to the manufacturer's instructions. Total RNA quality and quantity were controlled on an Agilent 2100 Bioanalyzer (Agilent). RNA-seq libraries were prepared using the TruSeq Stranded mRNA Sample Prep kit (Illumina) and sequenced on an Illumina GAIIx sequencer as 75-bp reads by Hybrigenics-Helixio.

Mapping Reads on the *Xenopus* Genome. Sequenced reads were assigned to each sample (unplexing) and adaptors were removed. The quality of the reads for each sample was checked using FastQC. The reads were then filtered based on their length, pairing, and quality, using Trimmomatic (version 0.32.1) (82). Cleaned reads were mapped to the *Xenopus* genome (JGI4.2 assembly) with Ensembl annotations (release 79) using Bowtie-0.12.7/TopHat 2 (version 0.6) software (83) (tophat.cbcb.umd.edu) (with a maximum intron size of 250,000 bp to discover novel junctions between exons).

Gene Expression Quantification and Differential Analysis. For each library, the Cufflinks (version 0.0.7) tool was applied to TopHat alignments to enumerate the number of short reads overlapping the Ensembl annotated genes (84). The Cuffmerge (version 0.0.6) script contained in Cufflinks was used to merge multiple assemblies from each sample. Gene transcription levels were computed from alignments carried out using TopHat 2 and compared statistically using the Cuffdiff (version 0.0.7) tool implemented in a Galaxy pipeline (https://galaxyproject.org). Genes were considered differentially transcribed when the transcription ratio TR (BaP or TCS treated/control) was >1.8 in either direction with an adjusted *P* value lower than 0.05 after multiple testing correction.

Functional Annotation Enrichment. Differentially expressed genes were subjected to annotation enrichment analysis and KEGG pathway mapping using the online functional annotation tool Database for Annotation, Visualization and Integrated Discovery (DAVID) (david.abcc.ncifcrf.gov/) (85), using all of the genes detected in our experiment as background (9,310 genes). *Xenopus* gene identifiers were transformed into their human orthologs to improve the richness of the output as previously described (41). The significance was calculated using a modified Fisher's exact test ($P < 0.05$). Heat maps of expression profiles for genes sharing enriched annotation pathways, or other genes associated with these pathways, were produced using TM4 MultiExperiment Viewer (MeV) software (86).

***Xenopus* Mating and Progeny Development.** At the end of the exposure period, five F_0 females and 10 F_0 males were selected from each exposure condition to naturally mate. Mating behavior was induced by two injections of human chorionic gonadotropin in the dorsal lymph sac of each *Xenopus* as previously described (87). After hatching, tadpoles were bred as described

above. F_1 development was characterized by the time from hatching to metamorphosis, together with the snout-vent length and weight at metamorphosis. At adult stage, F_1 animals were mated as described above.

ACKNOWLEDGMENTS. We thank Kim Barrett (Version Originale) and Oliver Ross (XpertScientific) for the English review of the revised manuscript. This work was funded by Communauté d'Universités et Établissements Université Grenoble–Alpes Initiatives de Recherche Stratégiques–Initiatives d'Excellence Grant and by the Federative Structure Environnemental and Systems Biology (BEeSy) of the Grenoble-Alpes University. C.R. received funding from the French Ministry of Higher Education and Research. M.U. was funded by the Région Auvergne–Rhône-Alpes.

1. Lips KR, Diffendorfer J, Mendelson JR, Sears MW (2008) Riding the wave: Reconciling the roles of disease and climate change in amphibian declines. *PLoS Biol* 6:e72.
2. Roelants K, et al. (2007) Global patterns of diversification in the history of modern amphibians. *Proc Natl Acad Sci USA* 104:887–892.
3. Hayes TB, Falso P, Gallipeau S, Stice M (2010) The cause of global amphibian declines: A developmental endocrinologist's perspective. *J Exp Biol* 213:921–933.
4. Carey C, Cohen N, Rollins-Smith L (1999) Amphibian declines: An immunological perspective. *Dev Comp Immunol* 23:459–472.
5. Kiesecker JM (2002) Synergism between trematode infection and pesticide exposure: A link to amphibian limb deformities in nature? *Proc Natl Acad Sci USA* 99:9900–9904.
6. World Health Organization (2012) *State of the Science of Endocrine Disrupting Chemicals*, eds Bergman A, Heindelerrold JJ, Jobling S, Kidd KA, Zoeller T (WHO, Geneva).
7. Fedorenkova A, et al. (2012) Ranking ecological risks of multiple chemical stressors on amphibians. *Environ Toxicol Chem* 31:1416–1421.
8. Kaplan M (October 29, 2009) Amphibians rarely give earliest warning of pollution. *Nature*, 10.1038/news.2009.1048.
9. Helbing CC (2012) The metamorphosis of amphibian toxicogenomics. *Front Genet* 3: 37.
10. Langlois VS, et al. (2010) Fadrozole and finasteride exposures modulate sex steroid- and thyroid hormone-related gene expression in *Silurana* (*Xenopus*) *tropicalis* early larval development. *Gen Comp Endocrinol* 166:417–427.
11. Crump D, Werry K, Veldhoen N, Van Aggelen G, Helbing CC (2002) Exposure to the herbicide acetochlor alters thyroid hormone-dependent gene expression and metamorphosis in *Xenopus laevis*. *Environ Health Perspect* 110:1199–1205.
12. Opitz R, et al. (2005) Description and initial evaluation of a *Xenopus* metamorphosis assay for detection of thyroid system-disrupting activities of environmental compounds. *Environ Toxicol Chem* 24:653–664.
13. Hammond SA, Veldhoen N, Helbing CC (2015) Influence of temperature on thyroid hormone signaling and endocrine disruptor action in *Rana* (*Lithobates*) *catesbeiana* tadpoles. *Gen Comp Endocrinol* 219:6–15.
14. Hayes TB, et al. (2010) Atrazine induces complete feminization and chemical castration in male African clawed frogs (*Xenopus laevis*). *Proc Natl Acad Sci USA* 107: 4612–4617.
15. Hayes T, et al. (2002) Herbicides: Feminization of male frogs in the wild. *Nature* 419: 895–896.
16. Duarte-Guterman P, Navarro-Martín L, Trudeau VL (2014) Mechanisms of crosstalk between endocrine systems: Regulation of sex steroid hormone synthesis and action by thyroid hormones. *Gen Comp Endocrinol* 203:69–85.
17. Hayes TB, et al. (2011) Demasculinization and feminization of male gonads by atrazine: Consistent effects across vertebrate classes. *J Steroid Biochem Mol Biol* 127: 64–73.
18. Fan W, et al. (2007) Atrazine-induced aromatase expression is SF-1 dependent: Implications for endocrine disruption in wildlife and reproductive cancers in humans. *Environ Health Perspect* 115:720–727.
19. Fan W, et al. (2007) Herbicide atrazine activates SF-1 by direct affinity and concomitant co-activators recruitments to induce aromatase expression via promoter II. *Biochem Biophys Res Commun* 355:1012–1018.
20. Hayes TB, et al. (2006) Characterization of atrazine-induced gonadal malformations in African clawed frogs (*Xenopus laevis*) and comparisons with effects of an androgen antagonist (cyproterone acetate) and exogenous estrogen (17beta-estradiol): Support for the demasculinization/feminization hypothesis. *Environ Health Perspect* 114: 134–141.
21. Hayes TB, et al. (2002) Hermaphroditic, demasculinized frogs after exposure to the herbicide atrazine at low ecologically relevant doses. *Proc Natl Acad Sci USA* 99: 5476–5480.
22. Urbatzka R, Bottero S, Mandich A, Lutz I, Kloas W (2007) Endocrine disrupters with (anti)estrogenic and (anti)androgenic modes of action affecting reproductive biology of *Xenopus laevis*: I. Effects on sex steroid levels and biomarker expression. *Comp Biochem Physiol C Toxicol Pharmacol* 144:310–318.
23. Cevasco A, et al. (2008) Endocrine disrupting chemicals (EDC) with (anti)estrogenic and (anti)androgenic modes of action affecting reproductive biology of *Xenopus laevis*: II. Effects on gonad histomorphology. *Comp Biochem Physiol C Toxicol Pharmacol* 147:241–251.
24. Orton F, Tyler CR (2015) Do hormone-modulating chemicals impact on reproduction and development of wild amphibians? *Biol Rev Camb Philos Soc* 90:1100–1117.
25. Säfholm M, Ribbenstedt A, Fick J, Berg C (2014) Risks of hormonally active pharmaceuticals to amphibians: A growing concern regarding progestagens. *Philos Trans R Soc Lond B Biol Sci* 369:20130577.
26. Casals-Casas C, Desvergne B (2011) Endocrine disruptors: From endocrine to metabolic disruption. *Annu Rev Physiol* 73:135–162.
27. Chevalier N, Fénichel P (2015) Endocrine disruptors: New players in the pathophysiology of type 2 diabetes? *Diabetes Metab* 41:107–115.
28. Chevalier N, Fénichel P (2015) Bisphenol A: Targeting metabolic tissues. *Rev Endocr Metab Disord* 16:299–309.
29. Chevalier N, Fénichel P (2016) Endocrine disruptors: A missing link in the pandemy of type 2 diabetes and obesity? *Presse Med* 45:88–97.
30. Jiang Y, et al. (2014) Mitochondrial dysfunction in early life resulted from perinatal bisphenol A exposure contributes to hepatic steatosis in rat offspring. *Toxicol Lett* 228:85–92.
31. Alonso-Magdalena P, et al. (2010) Bisphenol A exposure during pregnancy disrupts glucose homeostasis in mothers and adult male offspring. *Environ Health Perspect* 118:1243–1250.
32. Susiarjo M, et al. (2015) Bisphenol a exposure disrupts metabolic health across multiple generations in the mouse. *Endocrinology* 156:2049–2058.
33. US Environmental Protection Agency (2014) EDSP21 Dashboard—Endocrine Disruptor Screening Program for the 21st Century. Available at https://actor.epa.gov/edsp21/. Accessed April 10, 2018.
34. Hinther A, Bromba CM, Wulff JE, Helbing CC (2011) Effects of triclocarban, triclosan, and methyl triclosan on thyroid hormone action and stress in frog and mammalian culture systems. *Environ Sci Technol* 45:5395–5402.
35. Miyata K, Ose K (2012) Thyroid hormone-disrupting effects and the amphibian metamorphosis assay. *J Toxicol Pathol* 25:1–9.
36. Wang F, Liu F, Chen W, Xu R, Wang W (2018) Effects of triclosan (TCS) on hormonal balance and genes of hypothalamus-pituitary-gonad axis of juvenile male Yellow River carp (*Cyprinus carpio*). *Chemosphere* 193:695–701.
37. Zhou Z, Yang J, Chan KM (2017) Toxic effects of triclosan on a zebrafish (*Danio rerio*) liver cell line, ZFL. *Aquat Toxicol* 191:175–188.
38. US Environmental Protection Agency (2010) Endocrine disruptor screening program; second list of chemicals for tier 1 screening. *Federal Register*, ed US Environmental Protection Agency (Office of the Federal Register, National Archives and Records Administration, Washington, DC).
39. Petersen G, Rasmussen D, Gustavson K (2007) Study on enhancing the endocrine disrupter priority list with a focus on low production volume chemicals (European Commission, Brussels). Available at ec.europa.eu/environment/chemicals/endocrine/pdf/final_report_2007.pdf. Accessed June 4, 2001.
40. Regnault C, et al. (2016) Metabolic and immune impairments induced by the endocrine disruptors benzo[a]pyrene and triclosan in *Xenopus tropicalis*. *Chemosphere* 155:519–527.
41. Regnault C, et al. (2014) Impaired liver function in *Xenopus tropicalis* exposed to benzo[*a*]pyrene: Transcriptomic and metabolic evidence. *BMC Genomics* 15:666.
42. Olivares-Rubio HF, et al. (2015) Relationship between biomarkers and endocrine-disrupting compounds in wild *Girardnichthys viviparus* from two lakes with different degrees of pollution. *Ecotoxicology* 24:664–685.
43. Trapido M, Ingeborg V (1996) On polynuclear aromatic hydrocarbons contamination levels in the ecosystem of Lake Peipsi in the 1970s–1980s. *Hydrobiologia* 338:185–190.
44. Blair BD, Crago JP, Hedman CJ, Klaper RD (2013) Pharmaceuticals and personal care products found in the Great Lakes above concentrations of environmental concern. *Chemosphere* 93:2116–2123.
45. Lindström A, et al. (2002) Occurrence and environmental behavior of the bactericide triclosan and its methyl derivative in surface waters and in wastewater. *Environ Sci Technol* 36:2322–2329.
46. Canada H (2016) Guidelines for canadian drinking water quality: Guideline technical document—benzo[a]pyrene (Water, and Air Quality Bureau, Healthy Environments and Consumer Safety Branch, Health Canada, Ottawa).
47. World Health Organization (2003) Polynuclear aromatic hydrocarbons in drinking-water. Background document for development of WHO. *Guidelines for Drinking-Water Quality* (WHO, Geneva).
48. Koliaki C, et al. (2015) Adaptation of hepatic mitochondrial function in humans with non-alcoholic fatty liver is lost in steatohepatitis. *Cell Metab* 21:739–746.
49. Bulteau AL, Ikeda-Saito M, Szweda LI (2003) Redox-dependent modulation of aconitase activity in intact mitochondria. *Biochemistry* 42:14846–14855.
50. Yamaguchi K, et al. (2007) Inhibiting triglyceride synthesis improves hepatic steatosis but exacerbates liver damage and fibrosis in obese mice with nonalcoholic steatohepatitis. *Hepatology* 45:1366–1374.
51. Otoda T, et al. (2013) Proteasome dysfunction mediates obesity-induced endoplasmic reticulum stress and insulin resistance in the liver. *Diabetes* 62:811–824.
52. Kasuga M (2006) Insulin resistance and pancreatic beta cell failure. *J Clin Invest* 116: 1756–1760.
53. Takahashi Y, Fukusato T (2014) Histopathology of nonalcoholic fatty liver disease/nonalcoholic steatohepatitis. *World J Gastroenterol* 20:15539–15548.
54. Michurina SV, et al. (2016) Linagliptin alleviates fatty liver disease in diabetic *db/db* mice. *World J Diabetes* 7:534–546.
55. Petersen KF, et al. (2007) The role of skeletal muscle insulin resistance in the pathogenesis of the metabolic syndrome. *Proc Natl Acad Sci USA* 104:12587–12594.
56. Satyarengga M, Zubatov Y, Frances S, Narayanswami G, Galindo RJ (2017) Glycogenic hepatopathy: A complication of uncontrolled diabetes. *AACE Clin Case Rep* 3: e255–e259.
57. Pagliassotti MJ, Kim PY, Estrada AL, Stewart CM, Gentile CL (2016) Endoplasmic reticulum stress in obesity and obesity-related disorders: An expanded view. *Metabolism* 65:1238–1246.

58. Bensellam M, et al. (2016) Hypoxia reduces ER-to-Golgi protein trafficking and increases cell death by inhibiting the adaptive unfolded protein response in mouse beta cells. *Diabetologia* 59:1492–1502.
59. Bechmann LP, et al. (2012) The interaction of hepatic lipid and glucose metabolism in liver diseases. *J Hepatol* 56:952–964.
60. Burri L, Thoresen GH, Berge RK (2010) The role of PPARα activation in liver and muscle. *PPAR Res* 2010:542359.
61. Brismar K, Fernqvist-Forbes E, Wahren J, Hall K (1994) Effect of insulin on the hepatic production of insulin-like growth factor-binding protein-1 (IGFBP-1), IGFBP-3, and IGF-I in insulin-dependent diabetes. *J Clin Endocrinol Metab* 79:872–878.
62. Pei L, et al. (2006) NR4A orphan nuclear receptors are transcriptional regulators of hepatic glucose metabolism. *Nat Med* 12:1048–1055.
63. Naik A, Košir R, Rozman D (2013) Genomic aspects of NAFLD pathogenesis. *Genomics* 102:84–95.
64. Musso G, Gambino R, Cassader M (2013) Cholesterol metabolism and the pathogenesis of non-alcoholic steatohepatitis. *Prog Lipid Res* 52:175–191.
65. Mondul A, et al. (2015) PNPLA3 I148M variant influences circulating retinol in adults with nonalcoholic fatty liver disease or obesity. *J Nutr* 145:1687–1691.
66. Chen JL, Lu XJ, Zou KL, Ye K (2014) Krüppel-like factor 2 promotes liver steatosis through upregulation of CD36. *J Lipid Res* 55:32–40.
67. Nagaya T, et al. (2010) Down-regulation of SREBP-1c is associated with the development of burned-out NASH. *J Hepatol* 53:724–731.
68. Moyer BJ, et al. (2016) Inhibition of the aryl hydrocarbon receptor prevents Western diet-induced obesity. Model for AHR activation by kynurenine via oxidized-LDL, TLR2/4, TGFβ, and IDO1. *Toxicol Appl Pharmacol* 300:13–24.
69. Paul KB, Thompson JT, Simmons SO, Vanden Heuvel JP, Crofton KM (2013) Evidence for triclosan-induced activation of human and rodent xenobiotic nuclear receptors. *Toxicol In Vitro* 27:2049–2060.
70. Cave MC, et al. (2016) Nuclear receptors and nonalcoholic fatty liver disease. *Biochim Biophys Acta* 1859:1083–1099.
71. Di Croce L, Bruscalupi G, Trentalance A (1997) Independent responsiveness of frog liver low-density lipoprotein receptor and HMGCoA reductase to estrogen treatment. *Pflugers Arch* 435:107–111.
72. Schultz MM, Bartell SE, Schoenfuss HL (2012) Effects of triclosan and triclocarban, two ubiquitous environmental contaminants, on anatomy, physiology, and behavior of the fathead minnow (*Pimephales promelas*). *Arch Environ Contam Toxicol* 63: 114–124.
73. Chai L, Wang H, Zhao H, Deng H (2016) Chronic effects of triclosan on embryonic development of Chinese toad, *Bufo gargarizans*. *Ecotoxicology* 25:1600–1608.
74. Taft JD, Colonnetta MM, Schafer RE, Plick N, Powell WH (2018) Dioxin exposure alters molecular and morphological responses to thyroid hormone in *Xenopus laevis* cultured cells and prometamorphic tadpoles. *Toxicol Sci* 161:196–206.
75. Smith D (1987) Adult recruitment in chorus frogs: Effects of size and date at metamorphosis. *Ecology* 68:344–350.
76. De Vito J, Chivers D, Kiesecker J, Belden L, Blaustein A (1999) Effects of snake predation on aggregation and metamorphosis of Pacific treefrog (*Hyla regilla*) larvae. *J Herpetol* 33:504–507.
77. Hayes TB, et al. (2006) Pesticide mixtures, endocrine disruption, and amphibian declines: Are we underestimating the impact? *Environ Health Perspect* 114:40–50.
78. Garait B, et al. (2005) Fat intake reverses the beneficial effects of low caloric intake on skeletal muscle mitochondrial H_2O_2 production. *Free Radic Biol Med* 39:1249–1261.
79. Bulteau AL, Szweda LI, Friguet B (2002) Age-dependent declines in proteasome activity in the heart. *Arch Biochem Biophys* 397:298–304.
80. Dunnett CW (1955) A multiple comparison procedure for comparing several treatments with a control. *J Am Stat Assoc* 50:1096–1121.
81. Horthorn MA (2016) The two-step approach—a significant ANOVA F-test before Dunnett's comparisons against a control—is not recommended. *Commun Stat Theory Methods* 45:3332–3343.
82. Bolger AM, Lohse M, Usadel B (2014) Trimmomatic: A flexible trimmer for Illumina sequence data. *Bioinformatics* 30:2114–2120.
83. Trapnell C, Pachter L, Salzberg SL (2009) TopHat: Discovering splice junctions with RNA-seq. *Bioinformatics* 25:1105–1111.
84. Trapnell C, et al. (2012) Differential gene and transcript expression analysis of RNA-seq experiments with TopHat and Cufflinks. *Nat Protoc* 7:562–578.
85. Huang W, Sherman BT, Lempicki RA (2009) Bioinformatics enrichment tools: Paths toward the comprehensive functional analysis of large gene lists. *Nucleic Acids Res* 37: 1–13.
86. Saeed AI, et al. (2003) TM4: A free, open-source system for microarray data management and analysis. *Biotechniques* 34:374–378.
87. Showell C, Conlon FL (2009) Natural mating and tadpole husbandry in the western clawed frog *Xenopus tropicalis*. *Cold Spring Harb Protoc* 2009:pdb.prot5292.